Correcting pervasive errors in RNA crystallography through enumerative structure prediction

Fang-Chieh Chou[1], Parin Sripakdeevong[2], Sergey M Dibrov[3], Thomas Hermann[3] & Rhiju Das[1,2,4]

© 2012 Nature America, Inc. All rights reserved.

Three-dimensional RNA models fitted into crystallographic density maps exhibit pervasive conformational ambiguities, geometric errors and steric clashes. To address these problems, we present enumerative real-space refinement assisted by electron density under Rosetta (ERRASER), coupled to Python-based hierarchical environment for integrated 'xtallography' (PHENIX) diffraction-based refinement. On 24 data sets, ERRASER automatically corrects the majority of MolProbity-assessed errors, improves the average R_{free} factor, resolves functionally important discrepancies in noncanonical structure and refines low-resolution models to better match higher-resolution models.

Over the last decade, progress in RNA crystallography has revealed many three-dimensional structures of functional RNAs, providing powerful information for understanding their biological functions[1,2]. Nevertheless, RNA structures are typically solved at low diffraction resolution (>2.5 Å)[3]. A recent report by the Protein Data Bank (PDB) X-ray Validation Task Force noted the ubiquity of bond geometry errors, anomalous sugar puckers and backbone-conformer ambiguities in RNA crystallographic models, and recommended that assessment of these features be included in PDB validation and during peer review[4]. There is thus a critical need for efficient algorithms that can resolve ambiguities in existing and future RNA crystallographic models.

The difficulty of resolving RNA crystallographic errors is underscored by limitations in currently available computational tools. RNA backbone correction (RNABC)[5] and RNA constructed using rotameric nucleotides (RCrane)[3] can identify and fix backbone-conformer errors in some models. However, these methods anchor phosphates and bases to starting positions determined manually and thus only correct a subset of errors. Recent advances in Rosetta RNA *de novo* modeling[6–8] and electron density–guided protein modeling[9,10] have suggested that confident, high-accuracy structure prediction may be feasible if it is guided by experimental data. We present here a method termed ERRASER, which we integrated with PHENIX tools for diffraction-guided refinement. The protocol is based on exhaustively sampling each nucleotide's possible conformations and on scoring by the physically realistic Rosetta energy function supplemented with an electron density correlation score (**Supplementary Fig. 1**). Based on a benchmark of published crystallographic data sets and newly solved RNA structures, we report that this automated pipeline resolves the majority of geometric errors while retaining or improving correlation to diffraction data.

To measure the effectiveness of the ERRASER-PHENIX pipeline, we collected a test set of 24 crystal structures for RNA molecules ranging from small pseudoknots to entire ribosomal subunits (**Fig. 1** and **Supplementary Table 1**). We compared the effectiveness of our ERRASER protocol to that of RNABC and RCrane as well as PHENIX alone (**Table 1**). In the starting PDB-deposited structures, MolProbity tools revealed many potential errors in four classes: atom-atom steric clashes, high frequencies of outlier bond lengths or angles, 'non-rotameric' backbone conformations and potentially incorrect sugar puckers[11]. Although not all of these features are necessarily incorrect, high frequencies of such errors in medium-resolution to low-resolution

Table 1 | Average values for the validation results of the benchmark set

	Outlier bond (%)[a]	Outlier angle (%)[a]	Clash score[b]	Outlier backbone rotamer (%)[c]	Potentially incorrect pucker (%)[d]	R	R_{free}	Nucleotide similarity (%)[e]	Pucker similarity (%)[e]
PDB	0.53	1.18	18.03	18.8	5.0	0.210	0.256	64.9	91.5
PHENIX	0.01	0.03	10.79	15.2	2.4	0.199	0.244	71.7	96.4
RNABC-PHENIX	0.01	0	10.03	15.3	2.4	0.200	0.244	71.9	96.3
RCrane-PHENIX	0.003	0.12	10.12	10.3	1.0	0.207	0.252	74.1	95.8
ERRASER-PHENIX	0	0	7.04	7.9	0.2	0.199	0.244	80.5	97.0

[a]Bond lengths and angles with deviation > 4 s.d. compared to PHENIX ideal geometry[11]. [b]Serious clashes (atom pairs that have steric overlaps ≥ 0.4 Å) per 1,000 atoms[11]. [c]Assigned using RNA Ontology Consortium definition[12]. [d]Determined using a geometric criterion based on the distance between the glycosidic bond vector (C1–N1/9) and the following (3) phosphate[11]. [e]Comparison of refined low-resolution models to independent high-resolution models (**Supplementary Table 9**). Nucleotides in which the differences between all torsion angles were smaller than 40° were denoted 'similar'. Nucleotides in which torsion angle δ agreed to within 20° were assigned 'similar' puckers.

[1]Department of Biochemistry, Stanford University, Stanford, California, USA. [2]Biophysics Program, Stanford University, Stanford, California, USA. [3]Department of Chemistry and Biochemistry, University of California at San Diego, La Jolla, California, USA. [4]Department of Physics, Stanford University, Stanford, California, USA. Correspondence should be addressed to R.D. (rhiju@stanford.edu).

RECEIVED 26 SEPTEMBER; ACCEPTED 30 OCTOBER; PUBLISHED ONLINE 2 DECEMBER 2012; DOI:10.1038/NMETH.2262

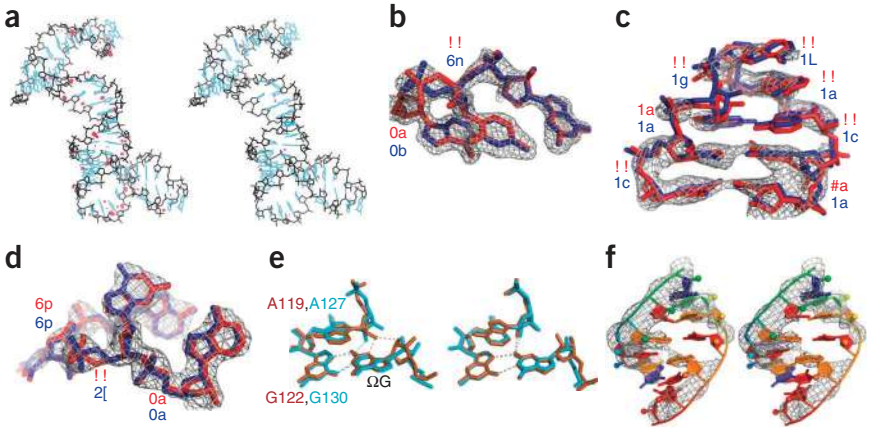

Figure 1 | Examples of geometric improvements by ERRASER-PHENIX. (**a**) Clash reduction in PDB structure 3R4F. Red dots, unfavorable clashes. Left, PDB data. Right, ERRASER-PHENIX data. (**b–d**) Backbone conformation improvement on nucleotides 62–64, chain A of PDB structure 1U8D (**b**), nucleotides 27–34, chain Q of PDB structure 2OIU (**c**) and nucleotides 33–36, chain A of PDB structure 2YGH (**d**). Rotamer assignments are shown as two-character codes at each suite[12]. '!!' stands for outlier rotamers. Red, PDB data. Blue, ERRASER-PHENIX data. (**e**) Functionally relevant pucker correction on group I ribozyme models. Brown, PDB 1Y0Q. Cyan, PDB 3BO3. Left, PDB data. Right, ERRASER-PHENIX data. (**f**) Base-pair geometry improvement on nucleotides 1–6 and 66–71, chain A of 3P49. Left, PDB data. Right, ERRASER-PHENIX data.

models (2.5–3.5 Å) compared to high-resolution models (<2.0 Å) suggest that most are due to inaccurate fits[3,5,11,12].

First, outlier bond lengths and angles (>4 s.d. from reference values) in the crystallographic models have mean frequencies of 0.53% and 1.18% in the starting PDB coordinates. Some of these outliers are due to different ideal bond geometries used by different refinement packages, and thus applying PHENIX alone lowered the outlier frequencies substantially. Nevertheless, application of ERRASER-PHENIX gave greater improvement, eliminating all the outlier bond lengths and angles in the benchmark (**Table 1** and **Supplementary Table 2**).

Second, ERRASER-PHENIX substantially reduced the steric clashes in RNA coordinates fitted into low-resolution electron density. In a bacteriophage prohead RNA test case (PDB identifier 3R4F), the initial pervasive clashes were reduced by 80% with ERRASER-PHENIX (**Fig. 1a**). Over the entire benchmark, the MolProbity clash score (number of serious clashes per 1,000 atoms[11]) was reduced from an average of 18.0 to 7.0 (**Fig. 2a**). Other refinement approaches that use less stringent or no steric criteria gave higher average clash scores (**Table 1** and **Supplementary Table 3**).

Third, a recent community-consensus analysis indicates that 92.4% of RNA backbone 'suites' (sets of two consecutive sugar puckers with five connecting backbone torsions) fall into 54 rotameric classes, many of which are correlated with unique functions[12]. Nonrotameric suites are thus potential fitting errors. ERRASER-PHENIX reduced the number of such outliers in 22 of 24 cases, and reduced the average outlier rate from 19% to 8% (**Table 1**, **Fig. 2b** and **Supplementary Table 4**). This result was notable because the 54-rotamer classification was not used during the Rosetta modeling. In high-resolution cases, the ERRASER-fitted conformer typically agreed better with the electron density as determined by visual inspection (**Fig. 1b**). For cases with medium to low resolution, where the starting and remodeled conformer fit the density equally well upon visual inspection, ERRASER-PHENIX gave substantially more rotameric conformers (**Fig. 1c**). As an additional test, we applied ERRASER during a recent RNA-puzzles blinded trial[13] involving a protein-RNA complex. ERRASER-PHENIX changed a suite in the protein-binding kink-turn in the starting RNA template (2YGH), from an outlier to the '2[' rotamer consistent with other kink-turn motifs[12] (**Fig. 1d**), which was indeed recovered in the subsequently released crystal structure (3V7E).

Fourth, RNA sugar rings typically exhibit either 2′-endo or 3′-endo conformations, but crystallographic assignments of these puckers can be ambiguous. Although sugar pucker errors can be confidently identified using simple geometric criteria, finding alternative error-free solutions remains difficult[11]. ERRASER-PHENIX reduced the mean pucker error rate from 5% to 0.2%, and gave zero pucker errors in 19 cases (**Table 1**, **Fig. 2c** and **Supplementary Table 4**). As an example with functional relevance, we fitted an adenosine in the active site of the group I ribozyme with different puckers in independent crystallographic models from bacteriophage Twort (adenosine 119 in 1Y0Q) and *Azoarcus* sp. BH72 (adenosine 127 in 3BO3). This discrepancy also led to different hydrogen bonding patterns between the adenosine's 2′-OH group and the guanosine (ΩG) substrate of the ribozyme (**Fig. 1e**). ERRASER-PHENIX improved agreement between the Twort and *Azoarcus* models throughout the active site and gave the same

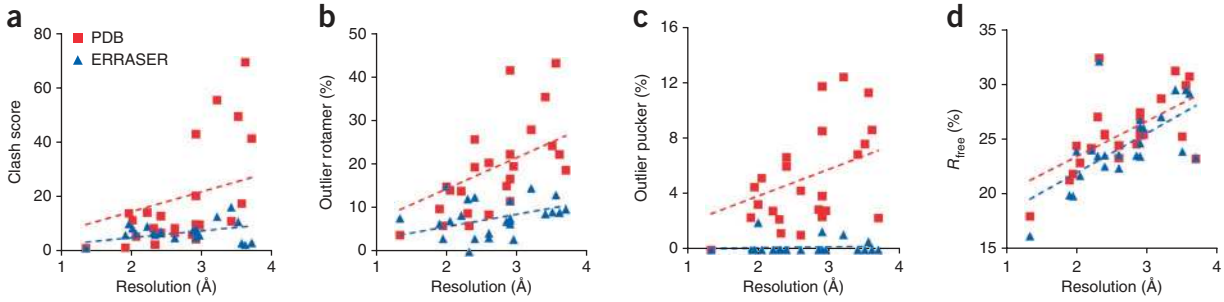

Figure 2 | Improvements of the crystallographic models by ERRASER-PHENIX across the test cases. (**a**) Clash score. (**b**) Frequencies of outlier backbone rotamers. (**c**) Frequencies of outlier puckers. (**d**) R_{free} factors. The dashed lines denote linear fits.

© 2012 Nature America, Inc. All rights reserved.

2′-endo pucker conformation and hydrogen-bonding network (**Fig. 1e**), in agreement with recent double-mutant analyses of group I ribozyme[14].

ERRASER-PHENIX also improved RNA base-pairing patterns with enhanced co-planarity and hydrogen-bonding geometry of interacting bases, as assessed by the automated base-pair assignment program MC-Annotate[15] and illustrated here for a glycine riboswitch (3P49, **Fig. 1f**). Furthermore, ERRASER-PHENIX led to remodeled glycosidic bond torsions (syn versus anti χ), whose accuracy we confirmed in several cases (**Supplementary Results**, **Supplementary Fig. 2** and **Supplementary Tables 5**, **6**).

We also evaluated the fits of our models to the diffraction data using R and R_{free} factors. Avoiding increases in R_{free}, the correlation to set-aside diffraction data, is critical for preventing overfitting of experimental data[16]. The ERRASER-PHENIX pipeline consistently decreased both R and R_{free}, lowering R_{free} in 22 of 24 cases. The average R factor dropped from 0.210 to 0.199 and average R_{free} factor dropped from 0.255 to 0.243 (**Table 1**, **Fig. 2d** and **Supplementary Tables 7**, **8**). Other methods gave the same or worse average R_{free}. As a practical demonstration, we had applied ERRASER-PHENIX to a newly solved structure of subdomain IIa from the hepatitis C virus internal ribosome entry site[17]. The ERRASER-PHENIX model gave fewer errors in all MolProbity criteria and lower R and R_{free}, and this model was therefore deposited into PDB as the final structure (3TZR).

As a separate independent assessment, we compared the similarity of remodeled low-resolution structures to original PDB-deposited models of high-resolution structures with the same sequences. We reasoned that pairs of models with the same sequences should give similar local conformations and that the higher-resolution models could be used as working references. For all 13 such cases (**Table 1** and **Supplementary Tables 9**, **10**), ERRASER-PHENIX remodeling gave low-resolution models with increased agreement in backbone torsions and sugar puckers to those in the deposited high-resolution models. In addition, we evaluated structures related by noncrystallographic symmetry or by internal homology and found that ERRASER improved their agreement in all tested cases (**Supplementary Results** and **Supplementary Tables 11**, **12**).

We also tested the quality improvement for lower-resolution models by ERRASER-PHENIX by comparing six data sets with low diffraction resolution (3.20–3.69 Å) to five data sets with high diffraction resolution (1.90–2.21 Å). For the low-resolution data sets, ERRASER-PHENIX improved the mean clash score from 40.8 to 7.9, which was lower than the mean clash score of 9.3 in the original high-resolution models. This value (7.9) is equal to the median clash score for models solved at 1.8 Å in a recent whole-PDB survey[4]. Similar reductions in outlier bond lengths and angles, outlier backbone rotamers and anomalous sugar puckers were apparent (**Supplementary Tables 2**–**4**).

For RNA crystallographic data sets across a wide range of resolutions and molecular size, ERRASER-PHENIX led consistent and substantial reduction of geometric errors, as assessed by independent validation tools and, in some cases, by independent functional evidence. The improved models gave similar or better fits to set-aside diffraction data in all cases. For all tested geometric features as well as R and R_{free} values, the ERRASER-remodeled coordinates were significantly improved compared to starting PDB values across the benchmark ($P < 0.02$ by Wilcoxon signed-rank test; **Supplementary Table 13**). Finally, comparison of remodeled low-resolution and independent high-resolution data sets indicated that this automated pipeline consistently increased the accuracy of RNA crystallographic models. We therefore expect this algorithm to mark an application of *ab initio* RNA three-dimensional structure prediction that will be widely useful in experimental biology. ERRASER is available in the current Rosetta release (3.4) at http://www.rosettacommons.org/, as an online application through the Rosetta online server that includes everyone (ROSIE; http://rosie.rosettacommons.org/) and as a part of the PHENIX package (http://www.phenix-online.org/).

METHODS

Methods and any associated references are available in the online version of the paper.

Note: Supplementary information is available in the online version of the paper.

ACKNOWLEDGMENTS

We thank J.S. Richardson for suggesting this problem and for detailed evaluation of the results we used to improve the program; C.L. Zirbel and N.B. Leontis for suggestions on base pair validation; B. Stoner and D. Herschlag for discussions on group I ribozyme active site; T. Terwilliger and J. Headd for aid in integrating ERRASER into PHENIX; S. Lyskov for setting up the ERRASER protocol on the ROSIE Server; members of the Das lab for comments on the manuscript; and members of the Rosetta and the PHENIX communities for discussions and code sharing. Computations were performed on the BioX^2 cluster (US National Science Foundation CNS-0619926) and the Extreme Science and Engineering Discovery Environment resources (US National Science Foundation OCI-1053575). This work was supported by funding from US National Institutes of Health (R21 GM102716 to R.D. and R01 AI72012 to T.H.), a Burroughs-Wellcome Career Award at Scientific Interface (R.D.), Governmental Scholarship for Study Abroad of Taiwan and Howard Hughes Medical Institute International Student Research Fellowship (F.-C.C.), and the C.V. Starr Asia/Pacific Stanford Graduate Fellowship (P.S.).

AUTHOR CONTRIBUTIONS

F.-C.C., P.S. and R.D. designed the research. F.-C.C. implemented the methods and analyzed the results. P.S. provided code and assisted in data analysis. S.M.D. and T.H. provided the starting model and diffraction data of the unreleased 3TZR structure and evaluated its refinement. F.-C.C. and R.D. prepared the manuscript. All authors reviewed the manuscript.

COMPETING FINANCIAL INTERESTS

The authors declare no competing financial interests.

Published online at http://www.nature.com/doifinder/10.1038/nmeth.2262. Reprints and permissions information is available online at http://www.nature.com/reprints/index.html.

1. Ban, N., Nissen, P., Hansen, J., Moore, P.B. & Steitz, T.A. *Science* **289**, 905–920 (2000).
2. Gesteland, R.F., Cech, T. & Atkins, J.F. (eds.). *The RNA World: The Nature of Modern RNA Suggests a Prebiotic RNA World*. 3rd edn. (Cold Spring Harbor Laboratory Press, 2006).
3. Keating, K.S. & Pyle, A.M. *Proc. Natl. Acad. Sci. USA* **107**, 8177–8182 (2010).
4. Read, R.J. *et al. Structure* **19**, 1395–1412 (2011).
5. Wang, X. *et al. J. Math. Biol.* **56**, 253–278 (2008).
6. Das, R. & Baker, D. *Proc. Natl. Acad. Sci. USA* **104**, 14664–14669 (2007).
7. Das, R., Karanicolas, J. & Baker, D. *Nat. Methods* **7**, 291–294 (2010).
8. Sripakdeevong, P., Kladwang, W. & Das, R. *Proc. Natl. Acad. Sci. USA* **108**, 20573–20578 (2011).
9. DiMaio, F., Tyka, M.D., Baker, M.L., Chiu, W. & Baker, D. *J. Mol. Biol.* **392**, 181–190 (2009).
10. DiMaio, F. *et al. Nature* **473**, 540–543 (2011).
11. Chen, V.B. *et al. Acta Crystallogr. D Biol. Crystallogr.* **66**, 12–21 (2010).
12. Richardson, J.S. *et al. RNA* **14**, 465–481 (2008).
13. Cruz, J.A. *et al. RNA* **18**, 610–625 (2012).
14. Forconi, M. *et al. Angew. Chem. Int. Edn.* **48**, 7171–7175 (2009).
15. Gendron, P., Lemieux, S. & Major, F. *J. Mol. Biol.* **308**, 919–936 (2001).
16. Brunger, A.T. *Nature* **355**, 472–475 (1992).
17. Dibrov, S.M. *et al. Proc. Natl. Acad. Sci. USA* **109**, 5223–5228 (2012).

© 2012 Nature America, Inc. All rights reserved.

ONLINE METHODS

Overview of the ERRASER-PHENIX pipeline. The ERRASER-PHENIX pipeline involves three major stages (**Supplementary Fig. 1a**). The starting model deposited in the PDB was first refined in PHENIX (v. dev-1034), with hydrogen atoms added. The refined model and electron-density map (setting aside the data for R_{free} factor calculations; see below) were then passed into Rosetta (version r50831) for a three-step real-space refinement. First, all torsion angles and all backbone bond lengths and bond angles were subjected to continuous minimization under the Rosetta high-resolution energy function supplemented with electron density correlation score. The Rosetta all-atom energy function models hydrogen bonding, Lennard-Jones packing, solvation and torsional preferences, and has been successful in the modeling and design of RNA at near-atomic accuracy[7,8]. The electron density score term is similar to the Rosetta electron density score recently pioneered for application to electron cryomicroscopy and molecular replacement[9,10]. Second, bond length, bond angle, pucker and suite outliers were identified using phenix.rna_validate. In addition, we also included nucleotides that shifted substantially during the initial Rosetta minimization (evaluated by nucleotide-wise r.m.s. deviation before and after minimization). These outlier and high–r.m.s. deviation nucleotides were rebuilt by single-nucleotide stepwise assembly (SWA) in a one-by-one fashion, where all of a nucleotide's atoms and the atoms up to the previous and next sugar were sampled by an exhaustive grid search of all torsions and a kinematic loop closure at sub-angstrom resolution (**Supplementary Fig. 1b**)[8,18]. If SWA found a lower-energy alternative structure of the rebuilt nucleotide, this new conformation was accepted. Third, the new model was minimized again in Rosetta. The rebuilding-minimization cycle was iterated three times to obtain the final ERRASER model. This model was again refined in PHENIX against diffraction data to obtain the final ERRASER-PHENIX model. All the ERRASER-PHENIX remodeled structures discussed in this paper are available as **Supplementary Data**.

The new Rosetta module, ERRASER. The ERRASER protocol consisted of three steps: an initial whole-structure minimization, followed by single-nucleotide rebuilding and finally another whole-structure minimization. Before passing the models into ERRASER, the PHENIX-generated PDB files were converted to the Rosetta format. Protein components, ligands and modified nucleotides were removed from the model because current enumerative Rosetta modeling only handles standard RNA nucleotides. To avoid anomalies in refitting, we held fixed the positions of the nucleotides that were bonded or in van der Waals contact with these removed atoms during the next ERRASER step. In 2OIU, a cyclic RNA structure, we also held fixed the first and the last nucleotides in the RNA chain to prevent the bonds from breaking during ERRASER. For structures that have notable interaction through crystal contacts, we manually included the interacting atoms in the ERRASER starting models.

Throughout the ERRASER refinement, an electron density score (unbiased by excluding set-aside R_{free} reflections during map creation; see below) was added to the energy function to ensure that the rebuilt structural models retained a reasonable fit to the experimental data. The electron density scoring in our method is slightly different from the one published recently[9,10]. Instead of calculating the density profile of the model every time we rescored the model, we precalculated the correlation between the density of a single atom and the experimental density in a fine grid. The score was defined as the negative of the sum of the atomic numbers of all the heavy atoms in the model times this rapidly computed real-space correlation coefficient. This new density scoring term, named 'elec_dens_atomwise', was an order of magnitude faster than the one in the previous Rosetta release, thus reducing the total computational time of our method substantially. To accommodate the change of our energy function caused by the electron density energy constraint, we also modified the weights in the original scoring function. The scoring weights file is included in the Rosetta release named 'rna_hires_elec_dens.wts'.

In addition, we used a new RNA torsional potential for this study. This new potential was obtained by fitting to the logarithm of the histogram of RNA torsions derived from the RNA11 data set (http://kinemage.biochem.duke.edu/databases/rnadb.php). The RNA11 data set contains 24,842 RNA suites and 311 different PDB entries, which is much richer and more diverse than the 50S ribosomal subunit model (1JJ2, 2,875 suites) used in deriving the original potential[7]. This new potential can be turned on by including the tag "-score:rna_torsion_potential RNA11_based_new" in the Rosetta command line.

During the whole-structure minimization, we constrained the phosphate atoms in the RNA to their starting position; this is especially important for low-resolution models where the phosphate positions were not accurately defined by electron density. Errors in phosphate positions were corrected during the latter rebuilding step. We also found that when the molecule was too large, Rosetta could not minimize the entire molecule because of slow scoring. Therefore for any molecule larger than 150 nucleotides, we decomposed the RNA into smaller segments with an automated script rna_decompose.py, and minimized each of them sequentially. To retain all interactions, we also included the nucleotides within 5 Å radius of the segment being minimized as fixed nucleotides during the minimization.

After the whole-structure minimization, we used PHENIX.rna_validate to analyze the obtained models. All nucleotides assigned to have outlier bond lengths, bond angles, puckers and/or potentially erroneous backbone rotamers (outliers or regular rotamers with suiteness < 0.1; suiteness is a quality measurement for rotamer assignments[12]) were identified as problematic and were rebuilt in subsequent Rosetta single-nucleotide rebuilding. Furthermore, because the single-nucleotide rebuilding region in Rosetta did not match the definition of a 'suite', we rebuilt both the selected nucleotide and the nucleotide preceding it to cover the whole suite for rotameric outliers.

In addition to rebuilding outlier nucleotides, we also computed the nucleotide-wise r.m.s. deviation between the models before and after minimization. The nucleotides with r.m.s. deviation larger than 0.05 times the diffraction resolution and within the 20% of the largest r.m.s. deviation nucleotides were also selected for rebuilding. We reasoned that because these nucleotides moved substantially after Rosetta minimization, their starting conformations were not favorable in terms of Rosetta energy function and were potentially erroneous.

The single-nucleotide rebuilding step used in our method was based on a modified SWA algorithm in which the RNA chain was closed using triaxial kinematic loop closure[18]. For nucleotides

© 2012 Nature America, Inc. All rights reserved.

doi:10.1038/nmeth.2262

at chain termini, the original SWA sampling was used because no chain closure was required. To rebuild nucleotides inside the RNA chain, we first created a chain break between O3′ and P in the lower suite of the rebuilding nucleotide. Then we sampled all possible torsion angles for ε_i, ξ_i, α_i, α_{i+1} in 20° steps, and the two most common conformation of the sugar pucker, 2′-endo and 3′-endo. For each sampled conformation, analytical loop closure was applied to close the chain and determined the remaining six torsions (β_i, γ_i, ε_i, ξ_i, β_{i+1}, γ_{i+1}), which formed three pairs of pivot-sharing torsions. The glycosidic torsion χ_i and the 2′-OH torsion $\chi_i^{2'\text{-OH}}$ were sampled after chain closure, and the generated models were further minimized in Rosetta. During the rebuilding, we applied a modest constraint to the glycosidic torsion so that it was more stable near the starting conformation; therefore only the base-orientation changes that gave substantial Rosetta energy bonuses were accepted as the final conformations. To reduce the computational expense, we only searched conformations that were within 3.0 Å r.m.s. deviation with respect to the starting models.

After the conformational search, 100 lowest-energy models were kept and additionally minimized under the constraint of the Rosetta 'linear_chainbreak' and 'chainbreak' energy term to ensure that the chain break was closed properly in the final model. Finally the best scored model was output as the new model for the RNA. If no new low-energy model could be found, then the program kept the starting model of that nucleotide. In the rebuilding process, the candidate nucleotides were rebuilt sequentially from the 5′ end to 3′ end of the RNA sequence. To speed up the Rosetta rebuilding process, the nucleotide being rebuilt was cut out from the whole structural model together with all nucleotides with at least one atom within a 5-Å radius, rebuilt using SWA and pasted back to the model.

After all the problematic nucleotides were rebuilt, we minimized the whole model again to reduce any bond-length or angle errors that might have occurred in the rebuilding process and to improve the overall energy of the model. In this study, the rebuilding-minimization cycle was iterated three times, although single iterations gave nearly equivalent results (data not shown). The coordinates of the RNA atoms in the PHENIX model were then substituted by the new coordinates in the Rosetta-rebuilt model to give the final ERRASER output.

The three ERRASER steps discussed above were wrapped into a python script erraser.py and can be performed automatically. The user needs to input a starting pdb file, a ccp4 map file, the resolution of the map and a list of any nucleotides that should be held fixed during refinement due to their interaction with removed atoms.

A sample ERRASER command line used for the refinement of PDB 3IWN dataset is shown below:

```
erraser.py -pdb 3IWN.pdb  -map 3IWN.ccp4
-map_reso 3.2 -fixed_res A37 A58-67 B137
B158-167
```

Here 3IWN.pdb is the name of the PHENIX refined model, 3IWN.ccp4 is the name of ccp4 density map file, -map_reso tag gives the resolution of the density map and -fixed_res specifies the nucleotides that should remain untouched. A37 means the 37th nucleotide of chain A in the pdb file.

Examples of the automatically generated Rosetta command lines by the python script are given in **Supplementary Notes**.

PHENIX refinement. PHENIX[19] (v. dev-1034) was used for all the refinements performed in this study. We first prepared the starting models downloaded from the PDB for refinement using phenix.ready_set. This step added missing hydrogen atoms into the models and set up constraint files including ligand constraints and metal coordination constraints. For ligands A23, 1PE and CCC, we substituted the PHENIX-generated ligand constraints with constraint files from the CCP4 monomer library to achieve better geometry. Furthermore, phenix.ready_set did not automatically create bond-length and bond-angle constraints at the linkage between some modified nucleotides (GDP and GTP) and standard nucleotides, or between the first and the last nucleotide of a cyclic RNA. In such cases these constraints were added manually. Finally, for pdb files with TLS (translation, libration, screw)[20] refinement records, the TLS group information was manually extracted from the pdb files and saved in a separate file for further use in PHENIX.

After all the files for the refinement were ready, a four-step PHENIX refinement was performed. In the first step, because PHENIX does not load in TLS records in the pdb files, we performed a one-cycle TLS refinement to recover the TLS information. Second, the models were refined by phenix.refine for three cycles. At this step, ADP (atomic displacement parameters) weight (wxu_scale) was optimized by PHENIX using a grid search, and other parameters were manually determined based on the criteria described below. For higher-resolution structures, a higher wxc_scale (scale for X-ray versus sterochemistry weight) was found to be appropriate. Based on initial tests (on PDB cases 1Q9A and 2HOP, which were not included in this paper's benchmark because they were used to set parameters), we used the following criteria: wxc_scale = 0.5 for resolution < 2.3 Å, wxc_scale = 0.1 for 2.3 Å ≤ resolution < 3 Å, wxc_scale = 0.05 for 3 Å ≤ resolution ≤ 3.6 Å and wxc_scale = 0.03 for resolution > 3.6 Å. The ordered_solvent option (automatic water updating) was turned on for all structures. Empirically, we found that the real-space refinement strategy in PHENIX only gave equal or worse *R* factor, so it was turned off throughout all the refinement steps in this study. TLS refinement was turned on only for structures with TLS records in the deposited PDB files. Third, the models were further refined in phenix.refine for nine cycles using the same parameter set. Fourth, the models were additionally refined in phenix.refine for three cycles, with all target weights (wxc_scale and wxu_scale) optimized during the run. Other parameters remained the same as in the first refinement round. Finally, we compared the models by the three different refinement steps and selected the one with the best fit to the diffraction data as the final model. For 3OTO, the multistep PHENIX refinement clearly distorted the starting model and gave worse geometries, so in this case we used the results obtained after the first refinement step. For 3P49, we supplied 1URN as a reference model to improve the protein part of the structure during refinement[21].

After the initial refinement, the electron density map was generated from the experimental diffraction data and the PHENIX refined structural model for further ERRASER improvement. We used phenix.maps to create $2mF_{\text{obs}} - DF_{\text{calc}}$ maps in ccp4 format, and diffraction data used for R_{free} validation were excluded for the map generation to avoid directly fitting to the R_{free} test set during ERRASER refinement. To avoid Fourier truncation errors resulting from the missing data, we filled any excluded or

© 2012 Nature America, Inc. All rights reserved.

missing F_{obs} values with F_{calc} values during the map calculation. The averaged kicked map approach was also used to reduce the noise and model bias of the maps[22].

The final PHENIX refinement, after the ERRASER steps, was similar to the starting refinement described above, with small variations. First, there was no need for an initial TLS refinement as the pdb files already had this information at this stage. Second, we ran phenix.ready_set again on the ERRASER model to generate metal coordination constraints for refinements, in case the new model presented different metal coordination patterns than the starting one. The models were then refined using PHENIX in the same multistep fashion, with the same parameter sets.

Examples of the PHENIX command lines used in this work are given in **Supplementary Notes**.

Refinement of 3TZR, a new structure of subdomain IIa from the hepatitis C virus IRES domain. The refinement of the 3TZR model currently deposited in the PDB was performed at an earlier stage of this work using an earlier PHENIX version (v1.7.1-743). The initial coordinates for 3TZR were already well-refined in PHENIX, and we therefore maintained the settings from that initial stage. In particular, during the PHENIX refinement, hydrogen atoms were not added to the model, and wxc_scale was set to 0.5. The final PHENIX refinement was performed using the same setting as the initial refinement.

***R* and R_{free} calculation.** For consistency, R and R_{free} values of all the models were calculated using phenix.model_vs_data[23]. For the starting models, the PHENIX-calculated R and R_{free} were generally similar to the values shown in the PDB header; both are reported in **Supplementary Tables 7**,**8**. In the main text, we reported PHENIX-calculated R and R_{free} to permit comparisons across the refinement benchmark.

Similarity analysis test. The similarities of the local geometries between similar structural models (**Supplementary Tables 9–12**) were evaluated as follows. If differences between the torsion angles (α, β, γ, δ, ε, ζ, χ) of each nucleotide pair were all smaller than 40°, the pair was counted as a similar nucleotide pair. If the difference of the δ angles of a nucleotide pair was smaller than 20°, the pair was assigned as having similar sugar pucker. Finally, r.m.s. deviations of all the torsion angles (in degrees) between the model pairs were calculated as an indicator of the model similarity in the torsional space.

Other tools. RNABC[5] (v1.11) and RCrane.CLI[3] (v1.01) were combined with PHENIX in the same manner as the ERRASER-PHENIX pipeline, by substituting the ERRASER stage with RNABC and RCrane, respectively. As RNABC rebuilt only one nucleotide per run, a python script was used to achieve automatic rebuilding of all nucleotides. The MolProbity[11] analysis was performed using command line tools phenix.clashscore and phenix.rna_validate in the PHENIX package. MC-Annotate[15] (v1.6.2) was used to assign base pairs in starting and refined models. All molecular images in this work were prepared using PyMol, except **Figure 1a**, which used MolProbity[11] and KiNG (Kinemage, Next Generation)[24].

18. Mandell, D.J., Coutsias, E.A. & Kortemme, T. *Nat. Methods* **6**, 551–552 (2009).
19. Adams, P.D. *et al. Acta Crystallogr. D Biol. Crystallogr.* **66**, 213–221 (2010).
20. Winn, M.D., Isupov, M.N. & Murshudov, G.N. *Acta Crystallogr. D Biol. Crystallogr.* **57**, 122–133 (2001).
21. Headd, J.J. *et al. Acta Crystallogr. D Biol. Crystallogr.* **68**, 381–390 (2012).
22. Praznikar, J., Afonine, P.V., Guncar, G., Adams, P.D. & Turk, D. *Acta Crystallogr. D Biol. Crystallogr.* **65**, 921–931 (2009).
23. Afonine, P.V. *et al. J. Appl. Cryst.* **43**, 669–676 (2010).
24. Chen, V.B., Davis, I.W. & Richardson, D.C. *Protein Sci.* **18**, 2403–2409 (2009).

© 2012 Nature America, Inc. All rights reserved.

doi:10.1038/nmeth.2262

Supplementary Information

Correcting pervasive errors in RNA crystallography through enumerative structure prediction

Fang-Chieh Chou, Parin Sripakdeevong, Sergey M. Dibrov, Thomas Hermann & Rhiju Das*

Supplementary Item	Title
Supplementary Figure 1	ERRASER-PHENIX algorithm.
Supplementary Figure 2	Base orientation improvements.
Supplementary Table 1	Benchmark test set of 24 structural models, sorted by resolution.
Supplementary Table 2	Outlier bond lengths and angles of the benchmark assessed by phenix.rna_validate.
Supplementary Table 3	Clashscore of the benchmark assessed by phenix.clashscore.
Supplementary Table 4	Outlier backbone rotamers and potentially incorrect sugar puckers of the benchmark assessed by phenix.rna_validate.
Supplementary Table 5	Number of base-pairs identified by MC-Annotate.
Supplementary Table 6	Summary of notable changes of base orientations (χ angle).
Supplementary Table 7	R factors of the benchmark.
Supplementary Table 8	R_{free} factors of the benchmark.
Supplementary Table 9	Similarity analysis between high-resolution and low-resolution models.
Supplementary Table 10	Torsional RMSDs (in degrees) between high-resolution and low-resolution models.
Supplementary Table 11	Similarity analysis for model pairs of the same or similar sequences.
Supplementary Table 12	Torsional RMSDs (in degrees) for model pairs of the same or similar sequences.
Supplementary Table 13	P-values of Wilcoxon signed-rank test between each method and the starting PDB dataset for all geometric features, R and R_{free}.
Supplementary Results	
Supplementary Notes	

Supplementary Figure 1. ERRASER-PHENIX algorithm. (**a**) Flow chart of the whole pipeline, the ERRASER steps are enclosed in red. (**b**) Enumerative RNA modeling in Rosetta steps. The blue torsions are explicitly sampled by enumeration and the green torsions are determined by automatic loop closure.

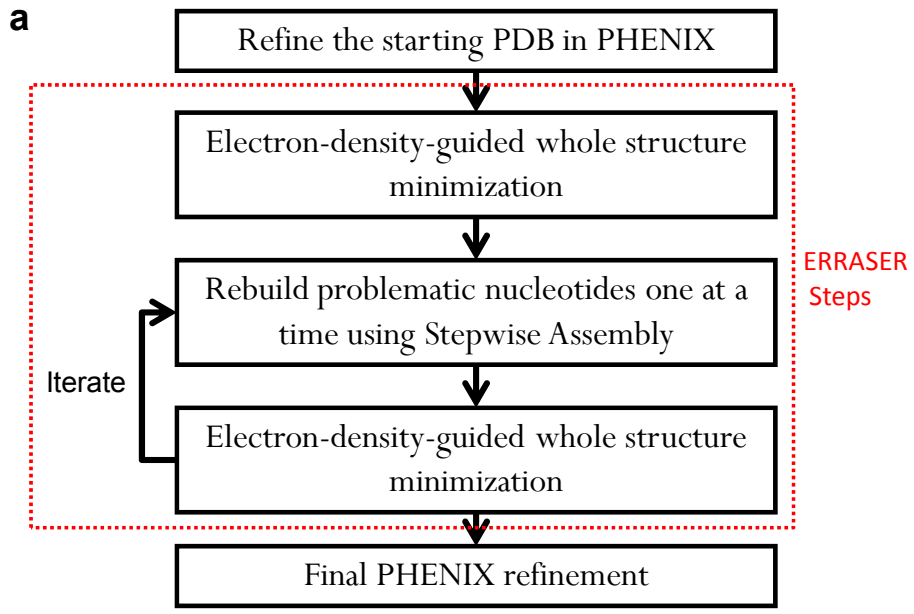

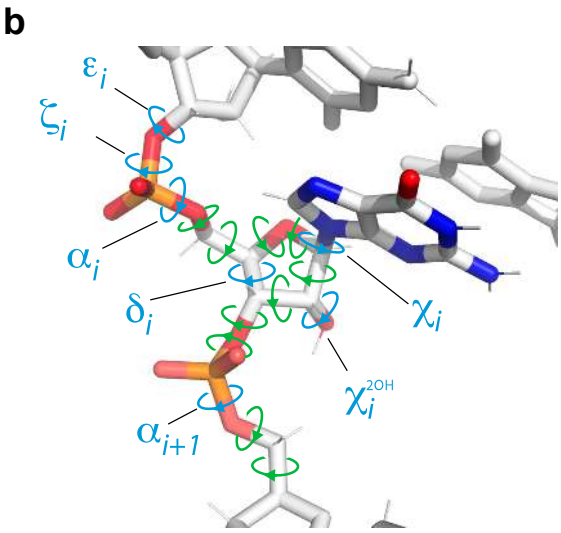

Supplementary Figure 2. Base orientation improvements. (**a**) Probability distribution of the χ angle in RNA09 (http://kinemage.biochem.duke.edu/databases/rnadb.php). The vertical lines show the range of syn vs. anti. Red: Purine; Blue: Pyrimidine; Dotted lines: 20X zoom-in of the distributions. (**b**) Base orientation changes in 2CKY, chain A, residue U35. Red: PDB model; Blue: ERRASER-PHENIX model; Brown: Reference model. **(c, d)** Base orientation changes in the ribosomal subunit 3OTO for residue **(c)** G266 and **(d)** U365. Red: PDB model; Blue: ERRASER-PHENIX model; Brown: Reference model (2VQE). Upper panel: Plot with electron density from 3OTO. Lower panel: Plot with electron density from 2VQE; the ERRASER model is aligned to the 2VQE model.

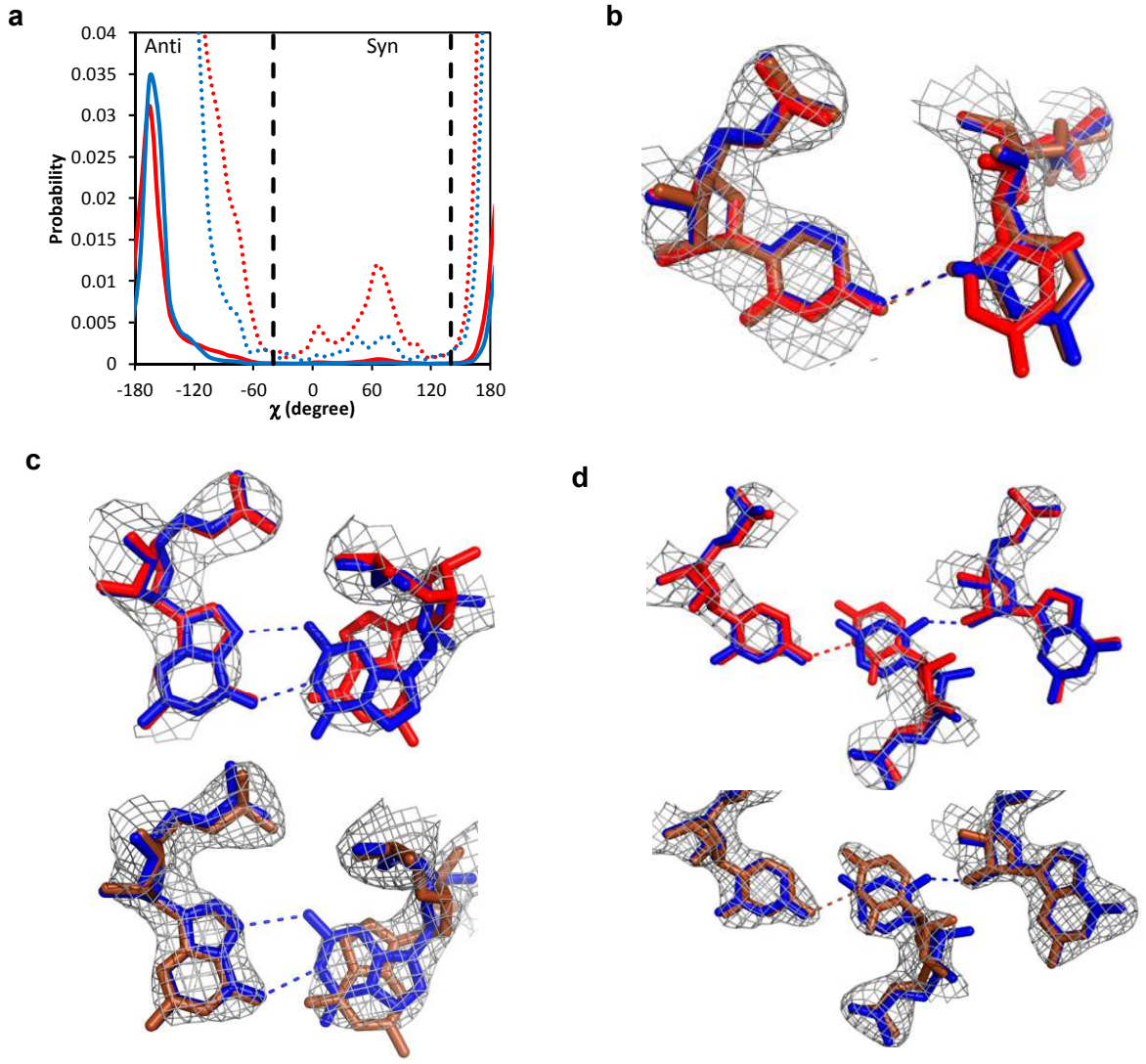

Supplementary Table 1. Benchmark test set of 24 structural models, sorted by resolution.

PDB ID	Name	RNA length[a]	Resolution (Å)
2A43	RNA Pseudoknot	26	1.34
3DIL	Lysine Riboswitch	174	1.9
1U8D	Guanine Riboswitch	68	1.95
3D2V	Eukaryotic TPP Riboswitch	77 × 2	2
2GDI	E. coli. TPP Riboswitch	80 × 2	2.05
3TZR	HCV IRES Subdomain IIa	36	2.21
3MXH	c-di-GMP Riboswitch	92	2.3
2PN4	HCV IRES Subdomain IIa	44 × 2	2.32
2QUS	Hammerhead Ribozyme	69 × 2	2.4
1Y27	Guanine Riboswitch	68	2.4
2OIU	L1 Ribozyme Ligase	71 × 2	2.6
2YGH	SAM-I Riboswitch	95	2.6
3DIZ	Lysine Riboswitch	174	2.85
3E5E	SAM-III Riboswitch	53	2.9
2GIS	SAM-I Riboswitch	94	2.9
2CKY	Eukaryotic TPP Riboswitch	77 × 2	2.9
2PN3	HCV IRES Subdomain IIa	44	2.9
3F2Q	FMN Riboswitch	112	2.95
3IWN	c-di-GMP Riboswitch	93 × 2	3.2
3BO3	*Azoarcus* Group I Ribozyme	212	3.4
3R4F	Prohead RNA	66	3.5
3P49	Glycine Riboswitch	169	3.55
1Y0Q	Twort Group I Ribozyme	233	3.6
3OTO	30S Ribosomal Subunit	1,522	3.69

[a] The length of RNA component of the molecule. "× 2" indicates 2 copies in the asymmetric unit.

Supplementary Table 2. Outlier bond lengths and angles of the benchmark assessed by phenix.rna_validate.

PDB ID	Outlier bonds(%)					Outlier angles(%)				
	PDB	PHENIX	RNABC-PHENIX	RCrane-PHENIX	ERRASER-PHENIX	PDB	PHENIX	RNABC-PHENIX	RCrane-PHENIX	ERRASER-PHENIX
2A43	0	0	0	0	0	0	0	0	0	0
3DIL	0	0	0	0	0	0	0	0	0	0
1U8D	0	0	0	0	0	2.99	0	0	0	0
3D2V	0	0	0	0	0	0	0	0	0	0
2GDI	0	0	0	0	0	0	0	0	0	0
3TZR	0	0	0	0	0	0	0	0	2.78	0
3MXH	0	0	0	0	0	0	0	0	0	0
2PN4	2.38	0	0	0	0	2.38	0	0	0	0
2QUS	1.47	0	0	0	0	3.68	0.74	0	0	0
1Y27	0	0	0	0	0	4.48	0	0	0	0
2OIU	2.11	0	0	0	0	0.7	0	0	0	0
2YGH	3.19	0	0	0	0	2.13	0	0	0	0
3DIZ	0	0	0	0	0	0	0	0	0	0
3E5E	1.92	0	0	0	0	0	0	0	0	0
2GIS	0	0	0	0	0	6.38	0	0	0	0
2CKY	1.3	0	0	0	0	0.65	0	0	0	0
2PN3	0	0	0	0	0	0	0	0	0	0
3F2Q	0	0	0	0	0	0	0	0	0	0
3IWN	0	0	0	0	0	4.3	0	0	0	0
3BO3	0.45	0	0	0	0	0	0	0	0	0
3R4F	0	0	0	0	0	0	0	0	0	0
3P49	0	0	0	0	0	0.59	0	0	0	0
1Y0Q	0	0	0	0	0	0	0	0	0	0
3OTO	0	0.2	0.27	0.07	0	0	0.07	0	0.13	0
Average	0.53	0.01	0.01	0.003	0	1.18	0.03	0	0.12	0
Avg. high-res[a]	0	0	0	0	0	0.60	0	0	0.56	0
Avg. low-res[b]	0.08	0.03	0.05	0.01	0	0.82	0.01	0	0.02	0
Equal to or better than PDB		23 / 24	23 / 24	23 / 24	24 / 24		23 / 24	24 / 24	22 / 24	24 / 24

Bond lengths and angles that have a deviation > 4 σ compared to PHENIX ideal geometry are counted as outliers.
[a] Average value for the five high resolution models 3DIL, 1U8D, 3D2V, 2GDI and 3TZR. Ultra-high resolution dataset 2A43 was excluded.
[b] Average value for the six lowest resolution models 3IWN, 3BO3, 3R4F, 3P49, 1Y0Q and 3OTO.

Supplementary Table 3. Clashscore of the benchmark assessed by phenix.clashscore.

PDB ID	PDB	PHENIX	RNABC-PHENIX	RCrane-PHENIX	ERRASER-PHENIX
2A43	1.19	1.19	2.38	2.38	1.19
3DIL	1.40	6.29	5.94	5.94	5.94
1U8D	14.02	16.22	13.59	12.71	10.08
3D2V	11.43	8.67	8.47	10.84	8.47
2GDI	5.52	8.41	8.98	8.60	6.50
3TZR	14.24	13.40	14.24	14.24	9.21
3MXH	8.48	5.58	6.69	8.93	6.92
2PN4	2.48	5.31	8.85	9.21	6.02
2QUS	12.97	13.43	10.52	12.75	6.71
1Y27	6.82	10.00	6.36	5.91	7.27
2OIU	8.48	7.61	7.61	9.13	5.00
2YGH	6.78	4.53	7.11	5.16	4.85
3DIZ	6.17	7.40	7.05	12.34	7.23
3E5E	4.51	4.53	2.83	9.07	5.09
2GIS	43.14	23.39	22.75	9.29	8.01
2CKY	20.47	12.99	11.22	10.83	7.68
2PN3	9.94	7.81	7.10	7.81	8.52
3F2Q	9.74	7.80	8.91	6.40	5.85
3IWN	55.65	23.31	19.63	13.94	12.71
3BO3	11.05	13.35	15.61	12.56	16.23
3R4F	49.62	16.07	15.12	16.54	10.85
3P49	17.56	5.43	6.57	7.43	3.00
1Y0Q	69.53	20.44	7.96	16.19	2.39
3OTO	41.42	15.75	15.30	14.69	3.17
Average	18.03	10.79	10.03	10.12	7.04
Avg. high-res[a]	9.32	10.60	10.24	10.47	8.04
Avg. low-res[b]	40.81	15.73	13.37	13.56	8.06
Equal to or better than PDB		15 / 24	17 / 24	15 / 24	17 / 24

Clashscore is the number of serious clashes (atom-pairs that have steric overlaps ≥ 0.4 Å) per 1,000 atoms.
[a] Average value for the five high resolution models 3DIL, 1U8D, 3D2V, 2GDI and 3TZR. Ultra-high resolution dataset 2A43 was excluded.
[b] Average value for the six lowest resolution models 3IWN, 3BO3, 3R4F, 3P49, 1Y0Q and 3OTO.

Supplementary Table 4. Outlier backbone rotamers and potentially incorrect sugar puckers of the benchmark assessed by phenix.rna_validate.

PDB ID	Outlier backbone rotamers					Potentially incorrect puckers				
	PDB	PHENIX	RNABC-PHENIX	RCrane-PHENIX	ERRASER-PHENIX	PDB	PHENIX	RNABC-PHENIX	RCrane-PHENIX	ERRASER-PHENIX
2A43	1	1	1	3	2	0	0	0	0	0
3DIL	17	13	14	11	11	4	2	1	0	0
1U8D	4	5	7	3	2	3	2	2	0	0
3D2V	23	25	26	18	23	5	2	2	2	3
2GDI	22	17	16	14	11	8	2	2	3	0
3TZR	5	5	5	3	3	1	1	1	0	0
3MXH	8	9	10	11	11	2	1	1	0	0
2PN4	5	2	1	1	0	1	0	0	0	0
2QUS	35	26	24	18	17	9	6	6	2	0
1Y27	13	10	8	2	2	4	2	2	0	0
2OIU	29	17	17	8	6	6	0	0	0	0
2YGH	8	7	8	5	3	1	0	0	0	0
3DIZ	26	19	17	11	12	5	1	1	0	0
3E5E	6	6	5	4	4	2	1	1	0	0
2GIS	21	16	20	14	6	8	7	7	1	0
2CKY	64	44	37	21	18	18	5	5	2	2
2PN3	7	2	2	2	3	1	0	0	0	0
3F2Q	21	15	15	9	3	3	2	2	2	0
3IWN	52	42	42	29	27	23	12	11	4	2
3BO3	78	70	63	22	19	15	6	6	1	0
3R4F	16	13	17	10	6	5	1	1	1	0
3P49	73	57	60	31	22	19	11	11	8	1
1Y0Q	52	59	58	55	21	20	14	11	8	0
3OTO	279	301	313	253	145	34	35	37	27	0
Average (%)[a]	18.8	15.2	15.3	10.3	7.9	5.0	2.4	2.4	1.0	0.2
Avg. high-res[b]	11.7	11.2	11.9	8.0	7.9	3.6	1.9	1.8	0.6	0.4
Avg. low-res[c]	28.6	25.6	26.4	16.6	10.7	8.1	4.3	4.0	2.3	0.3
Equal to or better than PDB		19 / 24	18 / 24	21 / 24	22 / 24		23 / 24	23 / 24	24 / 24	24 / 24

The backbone rotamer assignment is an effort of RNA Ontology Consortium[1]. Sugar pucker errors are determined using a geometric criterion based on the distance between the glycosidic bond vector (C1′–N1/9) and the following (3′) phosphate[2].

[a] Average error rate as percentage. Obtained by dividing the number of outliers with the total number of nucleotides.

[b] Average value for the five high resolution models 3DIL, 1U8D, 3D2V, 2GDI and 3TZR. Ultra-high resolution dataset 2A43 was excluded. The values are normalized by the numbers of nucleotides in the models.

[c] Average value (normalized) for the six lowest resolution models 3IWN, 3BO3, 3R4F, 3P49, 1Y0Q and 3OTO.

Supplementary Table 5. Number of base-pairs identified by MC-Annotate.

PDB ID	PDB	PHENIX	RNABC-PHENIX	RCrane-PHENIX	ERRASER-PHENIX
2A43	12	12	12	12	12
3DIL	88	89	89	90	91
1U8D	31	32	32	32	32
3D2V	69	68	68	69	68
2GDI	70	70	70	71	70
3TZR	15	15	15	15	15
3MXH	38	40	40	38	40
2PN4	32	32	32	32	32
2QUS	52	52	51	52	52
1Y27	36	34	35	34	36
2OIU	60	63	62	62	64
2YGH	37	37	37	39	43
3DIZ	88	89	89	89	88
3E5E	20	20	20	20	21
2GIS	40	36	38	37	40
2CKY	70	67	67	66	69
2PN3	16	17	16	16	16
3F2Q	43	44	44	44	44
3IWN	64	64	65	65	77
3BO3	86	85	81	85	92
3R4F	25	21	21	21	23
3P49	44	43	46	44	60
1Y0Q	97	89	87	92	104
3OTO	561	593	596	587	692
Average (%)[a]	83.4	82.7	82.7	82.8	87.0
Avg. high-res[b]	91.4	92.0	92.0	92.7	92.4
Avg. low-res[c]	72.2	69.4	69.3	70.1	81.5
Equal to or better than PDB		16 / 24	16 / 24	18 / 24	21 / 24

[a] Average value of (# of base-pairs) / (# of residues) × 2. The normalization is based on that the # of base-pairs in an ideal RNA duplex is half of the # of residues.
[b] Average value calculated for the five high resolution models 3DIL, 1U8D, 3D2V, 2GDI and 3TZR. Ultra-high resolution dataset 2A43 was excluded.
[c] Average value for the six lowest resolution models 3IWN, 3BO3, 3R4F, 3P49, 1Y0Q and 3OTO.

Supplementary Table 6. Summary of notable changes of base orientations (χ angle).

PDB ID	Resolution	Chain-Residue	Base Type	PDB		ERRASER-PHENIX		Reference PDB	Resolution	Chain-Residue	PDB	
				syn/anti	χ	syn/anti	χ				syn/anti	χ
3DIL[a]	1.9	A-110	G	syn	75	anti	-88	NA				
3D2V	2	B-35	U	syn	44	anti	-123	3D2V	2	A-35	anti	-110
2GDI	2.05	X-55	C	anti	-65	anti	-160	NA				
		Y-55	C	syn	52	anti	-135					
2QUS[b]	2.4	A-22	G	syn	97	anti	-78	NA				
		B-23	C	syn	56	anti	-119					
2OIU	2.6	P-19	U	syn	58	anti	-136	2OIU	2.6	Q-19	anti	-112
2YGH	2.6	A-14	A	syn	41	anti	-148	3GX5	2.4	A-9	anti	-85
3DIZ[a]	2.85	A-110	G	syn	80	anti	-85	NA				
2CKY	2.9	A-1	G	syn	-7	anti	174	3D2V	2	A-1	anti	-178
		A-35	U	syn	51	anti	-116			A-35	anti	-110
		A-74	U	syn	36	anti	-167			A-74	anti	-113
		B-67	C	syn	-39	anti	-129			B-67	anti	-100
		B-74	U	anti	-50	anti	-140			B-74	anti	-156
3IWN	3.2	A-7	C	anti	-51	anti	-162	3MXH	2.3	R-17	anti	-155
		A-33	A	anti	-100	syn	82			R-33	syn	67
3BO3	3.4	B-21	C	syn	91	anti	-150	NA				
3P49	3.55	A-731	C	anti	-58	anti	-152	NA				
		A-732	C	syn	-33	anti	-129					
1Y0Q[c]	3.6	A-35	A	anti	150	anti	-77	3BO3	3.4	NA		
		A-113	A	syn	21	anti	-176			B-121	anti	177
		A-158	A	syn	51	anti	-152			B-134	anti	-167
3OTO	3.69	A-91	C	anti	-58	anti	-164	2VQE	2.5	A-91	anti	-161
		A-108	G	syn	-11	anti	180			A-108	syn	3
		A-266	G	anti	-59	syn	54			A-266	anti	-83
		A-328	C	syn	116	anti	-85			A-328	syn	110
		A-346	G	syn	46	anti	-143			A-346	syn	61
		A-365	U	syn	43	anti	-157			A-365	syn	53
		A-421	U	syn	33	anti	-134			A-421	syn	6
		A-839	U	syn	72	anti	-164			A-839	syn	117
		A-1004	A	anti	-87	syn	67			A-1004	anti	-67
		A-1054	C	syn	81	anti	-139			A-1054	syn	77
		A-1279	A	syn	43	anti	-101			A-1279	syn	83

The table shows all the residues with $\Delta\chi > 90^{o}$ upon ERRASER-PHENIX refinement. The definition of syn and anti conformation is: syn: $-40 < \chi \leq 140$; otherwise is anti. See supplementary results for discussion.

[a] 3DIL and 3DIZ are structures of the same sequence with different resolution. However, ERRASER flipped residue 110 in both structure from syn to anti. Therefore we did not perform the high-resolution vs. low-resolution comparison in the table.

[b] For 2QUS, the backbone conformations for residue 22-23 for chain A and chain B, as well as the structures of nearby region, are quite different. Therefore we did not use the different chains as reference models in our analysis.

[c] 1Y0Q was compared to a homologous structure 3BO3. The two structures are group I ribozymes from different species. Residue 35 has no homologous partner in 3BO3 so was not compared.

Supplementary Table 7. *R* factors of the benchmark.

PDB ID	PDB (Deposited)	PDB (PHENIX calculated)	PHENIX	RNABC-PHENIX	RCrane-PHENIX	ERRASER -PHENIX
2A43	0.114	0.128	0.140	0.140	0.145	0.137
3DIL	0.192	0.183	0.172	0.169	0.171	0.170
1U8D	0.178	0.177	0.166	0.167	0.165	0.162
3D2V	0.207	0.202	0.212	0.210	0.224	0.211
2GDI	0.208	0.199	0.188	0.189	0.196	0.187
3TZR	0.182	0.182	0.184	0.185	0.188	0.180
3MXH	0.202	0.222	0.196	0.196	0.202	0.199
2PN4	0.261	0.258	0.264	0.270	0.268	0.264
2QUS	0.184	0.184	0.190	0.188	0.189	0.186
1Y27	0.232	0.224	0.204	0.205	0.207	0.203
2OIU	0.203	0.196	0.190	0.193	0.196	0.194
2YGH	0.200	0.186	0.197	0.206	0.199	0.205
3DIZ	0.193	0.200	0.198	0.201	0.203	0.202
3E5E	0.222	0.224	0.201	0.199	0.270	0.196
2GIS	0.266	0.249	0.216	0.219	0.218	0.216
2CKY	0.183	0.194	0.180	0.179	0.175	0.176
2PN3	0.229	0.214	0.213	0.212	0.239	0.210
3F2Q	0.200	0.197	0.199	0.202	0.202	0.200
3IWN	0.222	0.218	0.224	0.224	0.239	0.215
3BO3	0.282	0.266	0.244	0.240	0.274	0.239
3R4F	0.239	0.221	0.184	0.182	0.187	0.179
3P49	0.282	0.279	0.227	0.233	0.218	0.233
1Y0Q[a]	0.277	0.265	0.227	0.221	0.225	0.226
3OTO	0.173	0.177	0.163	0.164	0.163	0.186
Average	0.214	0.210	0.199	0.200	0.207	0.199
Avg. high-res[a]	0.193	0.188	0.185	0.184	0.189	0.182
Avg. low-res[b]	0.246	0.238	0.211	0.211	0.218	0.213
Equal to or better than PDB			16 / 24	15 / 24	12 / 24	16 / 24

[a] Average value for the five high resolution models 3DIL, 1U8D, 3D2V, 2GDI and 3TZR. Ultra-high resolution dataset 2A43 was excluded.
[b] Average value for the six lowest resolution models 3IWN, 3BO3, 3R4F, 3P49, 1Y0Q and 3OTO.

Supplementary Table 8. R_{free} factors of the benchmark.

PDB ID	PDB (Deposited)	PDB (PHENIX calculated)	PHENIX	RNABC-PHENIX	RCrane-PHENIX	ERRASER-PHENIX
2A43	0.190	0.180	0.166	0.165	0.176	0.162
3DIL	0.229	0.213	0.194	0.193	0.199	0.199
1U8D	0.228	0.218	0.198	0.202	0.202	0.198
3D2V	0.251	0.244	0.233	0.235	0.249	0.239
2GDI	0.241	0.229	0.216	0.219	0.219	0.217
3TZR	0.245	0.242	0.239	0.239	0.246	0.240
3MXH	0.239	0.270	0.231	0.233	0.239	0.235
2PN4	0.320	0.323	0.320	0.319	0.323	0.320
2QUS	0.253	0.253	0.235	0.231	0.234	0.225
1Y27	0.264	0.255	0.235	0.238	0.238	0.235
2OIU	0.238	0.233	0.224	0.225	0.225	0.224
2YGH	0.259	0.244	0.234	0.234	0.237	0.236
3DIZ	0.244	0.246	0.239	0.239	0.240	0.235
3E5E	0.259	0.258	0.254	0.256	0.348	0.261
2GIS	0.289	0.270	0.252	0.252	0.256	0.246
2CKY	0.250	0.253	0.236	0.235	0.231	0.234
2PN3	0.283	0.274	0.272	0.273	0.282	0.267
3F2Q	0.243	0.254	0.249	0.255	0.256	0.260
3IWN	0.292	0.287	0.282	0.281	0.297	0.270
3BO3	0.325	0.312	0.295	0.293	0.316	0.295
3R4F	0.271	0.252	0.245	0.241	0.243	0.239
3P49	0.310	0.299	0.290	0.279	0.280	0.295
1Y0Q	0.310	0.307	0.294	0.289	0.292	0.291
3OTO	0.231	0.232	0.225	0.225	0.223	0.233
Average	0.261	0.256	0.244	0.244	0.252	0.244
Avg. high-res[a]	0.239	0.229	0.216	0.218	0.223	0.219
Avg. low-res[b]	0.290	0.281	0.272	0.268	0.275	0.270
Equal to or better than PDB			24 / 24	24 / 24	17 / 24	21 / 24

[a] Average value for the five high resolution models 3DIL, 1U8D, 3D2V, 2GDI and 3TZR. Ultra-high resolution dataset 2A43 was excluded.
[b] Average value for the six lowest resolution models 3IWN, 3BO3, 3R4F, 3P49, 1Y0Q and 3OTO.

Supplementary Table 9. Similarity analysis between high-resolution and low-resolution models.

High res. models	Low res. models	Similar residues (%)[a]					Similar puckers (%)[b]				
		PDB	PHENIX	RNABC-PHENIX	RCrane-PHENIX	ERRASER-PHENIX	PDB	PHENIX	RNABC-PHENIX	RCrane-PHENIX	ERRASER-PHENIX
4FE5[c]	1U8D	87.5	87.5	87.5	89.1	92.2	98.4	96.9	96.9	98.4	100.0
4FE5[c]	1Y27	67.2	78.1	78.1	82.8	85.9	93.8	100.0	100.0	100.0	100.0
1U8D	1Y27	68.8	76.6	75.0	84.4	82.8	95.3	96.9	96.9	98.4	96.9
2YGH	2GIS	65.6	66.7	61.3	68.8	81.7	88.2	92.5	92.5	95.7	97.9
3DIL	3DIZ	94.3	93.7	92.5	85.1	94.8	98.9	98.9	98.9	98.9	98.3
3MXH	3IWN_1	53.3	54.6	55.8	61.0	71.4	85.7	92.2	92.2	89.6	94.8
3MXH	3IWN_2	45.5	49.4	48.1	50.7	63.6	81.8	90.9	90.9	89.6	90.9
3D2V_1	2CKY_1	57.1	71.4	72.7	66.2	79.2	85.7	96.1	96.1	94.8	97.4
3D2V_1	2CKY_2	42.9	64.9	67.5	74.0	75.3	89.6	97.4	97.4	97.4	94.8
3D2V_2	2CKY_1	54.6	61.0	62.3	63.6	77.9	92.2	100.0	100.0	98.7	100.0
3D2V_2	2CKY_2	45.5	59.7	64.9	68.8	71.4	90.9	98.7	97.4	97.4	97.4
2PN4_1	2PN3	77.3	84.1	81.8	86.4	86.4	95.5	97.7	97.7	93.2	97.7
2PN4_2	2PN3	84.1	84.1	86.4	81.8	84.1	93.2	95.5	95.5	93.2	95.5
Average		64.9	71.7	71.9	74.1	80.5	91.5	96.4	96.3	95.8	97.0
Equal to or better than PDB			12 / 13	11 / 13	11 / 13	13 / 13		12 / 13	12 / 13	12 / 13	12 / 13

[a] Nucleotide pair in which the differences between all torsion angles are smaller than 40°.
[b] Nucleotide pair in which the difference between δ angle is smaller than 20°.
[c] 4FE5 is a ultra-high resolution (1.32 Å) guanine riboswitch structure not in the benchmark set.

Supplementary Table 10. Torsional RMSDs (in degrees) between high-resolution and low-resolution models.

High res. models	Low res. models	PDB	PHENIX	RNABC-PHENIX	RCrane-PHENIX	ERRASER-PHENIX
4FE5	1U8D	25.1	24.5	25.8	21.5	15.3
4FE5	1Y27	39.3	36.7	33.5	33.2	30.5
1U8D	1Y27	37.3	35.1	32.0	30.3	31.4
2YGH	2GIS	38.4	37.7	38.2	32.2	29.0
3DIL	3DIZ	13.5	12.8	13.4	26.2	16.4
3MXH	3IWN_1	48.0	45.6	44.2	41.3	37.3
3MXH	3IWN_2	51.9	49.5	48.8	48.2	42.2
3D2V_1	2CKY_1	41.0	38.7	37.5	38.7	33.0
3D2V_1	2CKY_2	40.9	37.4	35.1	33.8	35.2
3D2V_2	2CKY_1	42.6	39.5	38.6	38.8	31.5
3D2V_2	2CKY_2	42.7	40.2	39.7	37.2	36.9
2PN4_1	2PN3	25.0	21.7	21.8	23.6	23.8
2PN4_2	2PN3	24.5	22.9	22.7	22.8	23.9
Average		36.2	34.0	33.2	32.9	29.7
Equal to or better than PDB			13 / 13	12 / 13	12 / 13	12 / 13

RMSD is calculated between all the torsion angles in the model pair.

Supplementary Table 11. Similarity analysis for model pairs of the same or similar sequences.

Chain1	Chain 2	Similar residues (%)[a]					Similar puckers (%)[b]				
		PDB	PHENIX	RNABC-PHENIX	RCrane-PHENIX	ERRASER-PHENIX	PDB	PHENIX	RNABC-PHENIX	RCrane-PHENIX	ERRASER-PHENIX
2GDI_1	2GDI_2	78.8	86.1	86.1	86.1	86.1	97.5	100.0	100.0	98.7	98.7
2OIU_1	2OIU_2	42.3	53.5	57.8	63.4	69.0	87.3	94.4	94.4	94.4	95.8
2QUS_1	2QUS_2	60.9	75.4	75.4	75.4	81.2	92.8	94.2	94.2	94.2	94.2
3P49_1	3P49_2	50.7	50.7	53.3	58.4	68.8	94.8	97.4	97.4	97.4	92.2
1U8D	1Y27	77.9	77.9	80.5	88.3	87.0	97.4	98.7	98.7	97.4	97.4
2YGH	2GIS	59.7	71.4	72.7	84.4	84.4	90.9	98.7	98.7	98.7	98.7
3DIL	3DIZ	86.4	90.9	88.6	90.9	90.9	97.7	97.7	97.7	97.7	97.7
3MXH	3IWN_1	34.2	39.5	34.2	68.4	73.7	84.2	94.7	92.1	94.7	100.0
3MXH	3IWN_2	68.8	78.1	82.8	85.9	84.4	95.3	100.0	100.0	100.0	100.0
3IWN_1	3IWN_2	65.6	71.0	66.7	71.0	89.3	88.2	93.6	93.6	95.7	97.9
3D2V_1	3D2V_2	94.3	95.4	94.8	92.5	97.7	98.9	100.0	100.0	100.0	100.0
3D2V_1	2CKY_1	53.3	55.8	54.6	64.9	72.7	85.7	92.2	92.2	92.2	96.1
3D2V_1	2CKY_2	45.5	48.1	49.4	55.8	62.3	81.8	92.2	92.2	93.5	90.9
3D2V_2	2CKY_1	57.1	70.1	70.1	77.9	85.7	85.7	98.7	98.7	98.7	98.7
3D2V_2	2CKY_2	42.9	64.9	70.1	79.2	77.9	89.6	100.0	100.0	100.0	97.4
2CKY_1	2CKY_2	54.6	63.6	64.9	79.2	83.1	92.2	100.0	100.0	98.7	98.7
2PN4_1	2PN4_2	45.5	62.3	64.9	77.9	74.0	90.9	98.7	98.7	97.4	100.0
2PN4_1	2PN3	77.3	81.8	79.6	84.1	81.8	95.5	97.7	97.7	93.2	97.7
2PN4_2	2PN3	84.1	84.1	86.4	93.2	86.4	93.2	95.5	95.5	95.5	95.5
Average		62.1	69.5	70.2	77.7	80.9	91.6	97.1	96.9	96.7	97.2
Equal to or better than PDB			19 / 19	19 / 19	18 / 19	19 / 19		19 / 19	19 / 19	18 / 19	18 / 19

[a] Nucleotide pair in which the differences between all torsion angles are smaller than 40°.
[b] Nucleotide pair in which the difference between δ angle is smaller than 20°.

Supplementary Table 12. Torsional RMSDs (in degrees) for model pairs of the same or similar sequences.

Chain 1	Chain 2	PDB	PHENIX	RNABC-PHENIX	RCrane-PHENIX	ERRASER-PHENIX
2GDI_1	2GDI_2	25.0	23.4	23.4	24.3	22.8
2OIU_1	2OIU_2	44.5	41.7	39.8	39.9	34.6
2QUS_1	2QUS_2	46.6	42.3	40.4	32.5	29.0
3P49_1	3P49_2	42.5	41.6	40.8	36.1	38.5
1U8D	1Y27	31.6	31.4	25.3	19.4	22.2
2YGH	2GIS	32.1	31.9	32.0	24.5	23.2
3DIL	3DIZ	19.2	17.5	22.4	17.7	16.4
3MXH	3IWN_1	50.9	49.7	51.7	37.0	32.9
3MXH	3IWN_2	37.3	34.4	26.0	28.2	28.8
3IWN_1	3IWN_2	38.4	37.4	37.5	30.5	22.1
3D2V_1	3D2V_2	13.5	12.0	11.7	19.5	11.7
3D2V_1	2CKY_1	48.0	45.6	44.0	38.0	37.3
3D2V_1	2CKY_2	51.9	49.4	46.7	42.1	42.5
3D2V_2	2CKY_1	41.0	38.5	35.1	31.4	27.6
3D2V_2	2CKY_2	40.9	36.9	30.8	27.3	31.9
2CKY_1	2CKY_2	42.6	39.6	37.8	27.5	24.9
2PN4_1	2PN4_2	42.7	40.3	37.8	27.5	31.0
2PN4_1	2PN3	25.0	21.2	26.7	24.1	22.2
2PN4_2	2PN3	24.5	21.3	20.0	16.5	20.2
Average		36.7	34.5	33.2	28.6	27.4
Equal to or better than PDB			19 / 19	16 / 19	18 / 19	19 / 19

RMSD is calculated between all the torsion angles in the model pair.

Supplementary Table 13. P-values of Wilcoxon signed-rank test between each method and the starting PDB dataset for all geometric features, R and R_{free}.

	Outlier bond	Outlier angle	Clashscore	Outlier backbone rotamer	Potentially incorrect pucker	Number of base-pairs	R	R_{free}
PHENIX	0.017	0.004	0.089	0.001	< 0.001	0.521	0.009	< 0.001
RNABC -PHENIX	0.017	0.005	0.045	0.007	< 0.001	0.394	0.024	< 0.001
RCrane -PHENIX	0.017	0.015	0.136	< 0.001	< 0.001	0.733	0.450	0.014
ERRASER -PHENIX	0.018	0.005	0.006	< 0.001	< 0.001	0.009	0.011	< 0.001

The Wilcocon signed-rank test is a non-parametric statistical test for pairs of related samples. The test can tell whether two datasets are significantly different from each other. Therefore it is suitable for the comparison between the PDB-deposited values and values after improvement methods. Here the two-sided P-value for each comparison is given in the table. All data in the benchmark (n = 24) are used for the analysis. Calculations are performed with the python library SciPy.

Supplementary Results

ERRASER-PHENIX improves RNA base-pairing geometry

ERRASER-PHENIX visually improved the base pairing patterns of the RNA models, enhancing the co-planarity of interacting bases. For example, Figure 1f shows a helical region in 3P49, a structure solved at 3.55 Å resolution. At this resolution, accurate positioning of base planes into the electron density map was difficult. Manual fits gave base pairs that were buckled or twisted compared to geometries seen in higher-resolution crystallographic models[3]. RNABC and RCrane held the base positions fixed during rebuilding and were thus unable to improve the base-pair planarity. On the other hand, ERRASER-PHENIX improved the planarity of the base-pairs, likely due to the hydrogen bonding potential included in the Rosetta energy function. Independent base-pair validation tools – which, like MolProbity, would permit unbiased assessment of improvement – are not currently available. However, we applied the base-pair assignment method MC-Annotate[4] and noted that the refined structures gave a higher number of automatically assigned base-pairs than the starting PDB models in 21 out of 24 cases (Supplementary Table 5). For the 3P49 case, ERRASER-PHENIX increased the number of base-pairs from 44 in the PDB model to 60. Other methods (RNABC-PHENIX and RCrane-PHENIX) lead to smaller improvements in this case, giving 46 and 44 base-pairs respectively.

ERRASER-PHENIX improves the base orientation

In addition to the base-pairing geometry improvement described above, ERRASER also improved the orientation of bases in the models. The glycosidic torsions in a RNA structure predominantly adopt two distinct conformations: syn and anti[5]. These two conformations can be distinguished by the value of χ torsion angle of the glycosidic bond. In the discussion below, the

syn conformation is defined as -40º < $\chi \leq$ 140º, and the remaining angle ranges are defined as anti, based on the distribution of χ angles in RNA09 dataset (Supplementary Fig. 2a, http://kinemage.biochem.duke.edu/databases/rnadb.php). It is also evident that the anti conformation is much more probable than syn conformation, and syn pyrimidine conformers are especially rare. Therefore in the current single-nucleotide rebuilding scheme, syn pyrimidine conformers were sampled only if the starting model adopts syn conformation. Supplementary Table 6 summarized all the notable base orientation changes ($\Delta\chi$ > 90 º) in the benchmark. While most of the changes are syn-to-anti flips, in agreement with the higher frequency of anti conformations, there are still a few anti-to-syn flips, confirming that ERRASER did not blindly flip the base orientation from syn to anti. To evaluate the confidence of these remodeled bases, these changes were compared to reference models of similar or higher resolution with same or similar sequence. If such models were not available, and there were two different copies of structures in one asymmetric unit, the different copy (to which the target nucleotide did not belong) was used as reference model. For all test cases where reference models are available except for the ribosome, all 12 base orientation changes agreed well with the reference. In some cases these orientation changes even introduced extra hydrogen bonds, further supporting these fixes (Supplementary Fig. 2b). For the lowest-resolution ribosome test case (3OTO, 3.69 Å), most of the conformational changes did not match the higher-resolution reference model (2VGE, 2.5 Å). However, since both structures were solved using molecular replacement, it is possible that the two deposited structures inherited the same base orientations from an earlier model[6-7], therefore might share the same erroneous conformations. By detailed inspection of the conformational changes, we found that the ERRASER changes in 3OTO gave the same or more hydrogen bonds as the starting coordinates and agreed well with the electron

density. For example, Supplementary Figure 2c shows an example of such an orientation change where a guanosine flipped from anti to syn and forming a Watson-Crick vs. Hoogsten base-pair with two extra hydrogen bonds. The density map of higher-resolution model did not falsify the possibility of this new, energetically more favorable conformation. On the other hand, Supplementary Figure 2d demonstrates a case where the flipping is ambiguous, where a uridine flipped from syn to anti, and both conformations have one hydrogen bond with nearby nucleotide. Although the starting conformation fits slightly better in the higher-resolution density map visually, it is possible that the alternative conformation also existed in the crystal structure with a smaller occupancy. Across the benchmark, ERRASER-PHENIX gave improved, or at least alternatively possible, conformations for the base orientations in RNA.

Pairwise comparison for models with similar sequences

Analogous to the independent comparison between remodeled low-resolution and original high-resolution models (see the main text), we reasoned that pairs of models with the same or similar RNA sequences should give similar conformations at corresponding nucleotides, and an accurate refinement procedure should maintain or improve this similarity. We drew 19 such structural pairs from three categories: models of the same sequences determined independently at different resolutions (11 cases, same pairs as those used in high-res vs. low-res comparisons); two copies present in the asymmetric unit related by non-crystallographic symmetry (7 cases); and the conserved regions of two aptamer domains in glycine riboswitch (1 case). Supplementary Table 10-11 summarizes the results of the similarity comparison of the torsion angles of each nucleotide pair, sugar pucker assignment and the RMSD in torsional space for these structure pairs. In nearly all cases, ERRASER-PHENIX improved these metrics compared to the PDB models, and gave better average values than RNABC-PHENIX and RCrane-PHENIX.

Supplementary Notes

Example Rosetta command lines used in ERRASER-PHENIX

(1) Full structure minimization.

```
erraser_minimizer.<exe> -native <input pdb> -out_pdb <output
pdb> -score::weights rna/rna_hires_elec_dens -
score:rna_torsion_potential RNA11_based_new –constrain_P true -
vary_geometry true -fixed_res <fixed residue list> -
edensity:mapfile <map file> -edensity:mapreso 2.0 -
edensity:realign no
```

(2) Single nucleotide rebuilding with analytical chain closure.

```
swa_rna_analytical_closure.<exe> -algorithm rna_resample_test -s
<input pdb> -native <native pdb> -out:file:silent blah.out -
sampler_extra_syn_chi_rotamer true -
sampler_extra_anti_chi_rotamer true -constraint_chi true -
sampler_cluster_rmsd 0.1 -sampler_native_rmsd_screen true -
sampler_native_screen_rmsd_cutoff 3.0 -sampler_num_pose_kept 100
-PBP_clustering_at_chain_closure true -
allow_chain_boundary_jump_partner_right_at_fixed_BP true -
add_virt_root true - rm_virt_phosphate true -sample_res 2 -
cutpoint_closed 2  -fasta fasta -input_res 1 3-4 -fixed_res 1 3-
4 -jump_point_pairs NOT_ASSERT_IN_FIXED_RES 1-4 -alignment_res
1-4 -rmsd_res 4 -score:weights rna/rna_hires_elec_dens -
edensity:mapfile <map file> -edensity:mapreso 2.0 -
edensity:realign no -score:rna_torsion_potential RNA11_based_new
```

(3) Single nucleotide rebuild at terminal nucleotides.

```
swa_rna_main.<exe> -algorithm rna_resample_test -s <input pdb> -
native <native pdb> -out:file:silent blah.out -
sampler_extra_syn_chi_rotamer true -
sampler_extra_anti_chi_rotamer true -constraint_chi true -
sampler_cluster_rmsd 0.1 -sampler_native_rmsd_screen true -
sampler_native_screen_rmsd_cutoff 3.0 -sampler_num_pose_kept 100
-PBP_clustering_at_chain_closure true -
allow_chain_boundary_jump_partner_right_at_fixed_BP true -
add_virt_root true - rm_virt_phosphate true -sample_res 2 -
cutpoint_closed 2 -fasta fasta -input_res 1-4 -fixed_res 2-4 -
jump_point_pairs NOT_ASSERT_IN_FIXED_RES 1-4 -alignment_res 1-4
```

```
-rmsd_res 4 -score:weights rna/rna_hires_elec_dens -
edensity:mapfile <map file> -edensity:mapreso 2.0 -
edensity:realign no -score:rna_torsion_potential RNA11_based_new
```

Example PHENIX command lines used in ERRASER-PHENIX

(1) phenix.ready_set.

```
phenix.ready_set 3E5E.pdb
```

(2) One-cycle TLS refinement.

```
phenix.refine 2QUS-sf.mtz 2QUS.updated.pdb GTP.cif
2QUS.metal.edits 2QUS.link.edits tls.params
main.number_of_macro_cycles=1 strategy=tls
```

(3) Three-cycle refinement with manual parameter set.

```
phenix.refine 2GIS-sf.mtz  2GIS.pdb  2GDI.metal.edits
ordered_solvent=true  optimize_adp_weight=true
strategy=individual_sites+individual_adp+occupancies
main.number_of_macro_cycles=3 wxc_scale=0.1
```

(4) Three-cycle refinement with automatically optimized target weight.

```
phenix.refine 2GIS-sf.mtz
2GIS_phenix_erraser_refine_001_refine_001.pdb
2GIS_phenix_erraser_refine_001_refine_001.metal.edits
ordered_solvent=true optimize_adp_weight=true
strategy=individual_sites+individual_adp+occupancies
main.number_of_macro_cycles=3 optimize_xyz_weight=true
```

(5) Density map creation.

```
phenix.maps maps.params

maps.params:
...
   map {
     map_type = 2mFo-DFc
     format = xplor *ccp4
     file_name = 2GIS_cell.ccp4
```

```
      kicked = True
      fill_missing_f_obs = True
      grid_resolution_factor = 1/4.
      region = selection *cell
      atom_selection = None
      atom_selection_buffer = 3
      sharpening = False
      sharpening_b_factor = None
      exclude_free_r_reflections = True
      isotropize = True
    }
...
```


1. Richardson, J.S. et al. RNA backbone: Consensus all-angle conformers and modular string nomenclature (an RNA Ontology Consortium contribution). *RNA* **14**, 465-481 (2008).
2. Chen, V.B. et al. MolProbity: all-atom structure validation for macromolecular crystallography. *Acta Cryst. D* **66**, 12-21 (2010).
3. Stombaugh, J., Zirbel, C.L., Westhof, E. & Leontis, N.B. Frequency and isostericity of RNA base pairs. *Nucleic Acids Res.* **37**, 2294-2312 (2009).
4. Gendron, P., Lemieux, S. & Major, F. Quantitative analysis of nucleic acid three-dimensional structures. *J. Mol. Biol.* **308**, 919-936 (2001).
5. Bloomfield, V.A. et al. Nucleic Acids: Structures, Properties, and Functions. (University Science Books, 2000).
6. Demirci, H. et al. Modification of 16S ribosomal RNA by the KsgA methyltransferase restructures the 30S subunit to optimize ribosome function. *RNA* **16**, 2319-2324 (2010).
7. Kurata, S. et al. Modified Uridines with C5-methylene Substituents at the First Position of the tRNA Anticodon Stabilize U·G Wobble Pairing during Decoding. *J. Biol. Chem.* **283**, 18801-18811 (2008).